On-Line Studies and Computer Simulation of the Melt Spinning of Nylon-66 Filaments

KENNETH F. ZIEMINSKI and JOSEPH E. SPRUIELL,
Department of Materials Science and Engineering, and Center for Materials Processing, University of Tennessee, Knoxville, Tennessee 37996-2200

Synopsis

A mathematical model was developed to describe the high-speed melt-spinning behavior crystallizable polymers. This model included the effects of acceleration, gravity, and air friction on the kinematics of the process; temperature and molecular orientation on the crystallization kinetics of the polymer; and temperature, molecular weight, and crystallinity on the elongational viscosity of the material. Experimental on-line diameter, birefringence, and temperature profiles were obtained for a 12,000 Mn nylon-66 at 2.5 g/min spun at take-up speeds ranging from 2800 to 6600 m/min. These profiles were qualitatively and reasonably quantitatively in agreement with the predicted profiles. They indicated that orientation induced crystallization occurs at spinning speeds greater than 4000 m/min. The experimental diameter and birefringence profiles were compared to those predicted by the model using Avrami indices of 3, 2, and 1. There was a small increase in the crystalline index at the lower speeds with decreasing index. The effect of the strain hardening was more significant at the higher speeds, this being shown by decreasing the exponent in the relationship for the crystallinity on the elongational viscosity. The model developed in this study indicates that high spinning speeds provide the high stress environment that increases the molecular orientation within the fiber. It is this higher molecular orientation that is the driving force for rapid crystallization on the spinline. This rapid crystallization causes a strain hardening, preventing any further drawdown in the fiber diameter and an abrupt rise in the birefringence. This behavior closely corresponds to the observed spinline profiles.

INTRODUCTION

The commercial development of high-speed melt-spinning technology has led to renewed interest in the fundamentals of the spinning process. There have been a number of attempts to mathematically model the melt-spinning process, but until recently, they have been limited to amorphous materials or to slowly crystallizing materials spun at speeds where no crystallization takes place in the spinline.[1-12] Recently, Katayama and Yoon[13] and Shimizu et al.[14] have developed models that include the effect of crystallization, and have applied these models to the melt spinning of poly(ethylene terephthalate) (PET). In the present work a mathematical model similar to that described by Shimizu et al.[14] has been further developed and applied to the simulation of the melt spinning of nylon 66. The results of the simulation have been compared to experimental measurements of diameter, temperature, and birefringence profiles made on the running spinline.

The model includes the effects of acceleration, air drag, and gravity on the process dynamics, and the effects of temperature and amorphous molecular orientation on the crystallization kinetics. The on-line measurements represent the most extensive on-line results yet reported for nylon 66.

Journal of Applied Polymer Science, Vol. 35, 2223–2245 (1988)
 CCC 0021-8995/88/082223-23$04.00

DESCRIPTION OF THE MATHEMATICAL MODEL

The mathematical model was developed from the equations of continuity, momentum, and energy by applying the kinematics of melt spinning and the following assumptions:

1. Steady State
2. No radial variations
3. The tangential and radial velocities, V_θ and V_r, are zero
4. The surface tension of the polymer air interface, F_{surf}, is negligible
5. Viscous heating is negligible
6. Conduction and radiation are negligible

This led to the following set of working relationships;

$$\frac{dF_{rheo}}{dz} = \frac{dF_{inert}}{dz} + \frac{\delta F_{drag}}{\delta z} - \frac{\delta F_{grav}}{\delta z} \tag{1}$$

where

$$\frac{dF_{inert}}{dz} = W\frac{dV}{dz} \tag{2}$$

$$\frac{\delta F_{drag}}{\delta z} = \rho C_d V^2 \pi D \tag{3}$$

$$\frac{\delta F_{grav}}{\delta z} = \frac{Wg}{V} \tag{4}$$

and

$$\frac{dT}{dz} = \frac{\pi Dh(T_a - T)}{WC_p} + \frac{\Delta H\, d\theta}{C_p\, dz} \tag{5}$$

A complete list of all symbols used herein is presented in the Appendix. Units consistent with the numerically quoted quantities are also given.

In order to apply these relationships to the melt-spinning process, expressions for the drag coefficient, heat transfer coefficient, molecular orientation, and crystallization kinetics were needed. The drag coefficient was derived by Sakiadis[15] from boundary layer theory as

$$C_d = 4/\beta\,\mathrm{Re} \tag{6}$$

where Re is the Reynolds number and β is a coefficient determined by integration from 0 to β of

$$\psi^2 = 8\int_0^\beta \frac{(z-1)\exp(2z) + z^2 + 1}{z^2}\,dz \tag{7}$$

where the parameter ψ is determined from

$$\psi^2 = 64z/D\,\mathrm{Re} \tag{8}$$

where Re is the Reynolds number based on fiber diameter and velocity.

The heat transfer coefficient used was that proposed by Kase and Matsuo[3]

$$h = 6.85 \times 10^{-5}(\rho V^2/W)^{0.259} \tag{9}$$

for spinning without transverse air flows.

The orientation of the amorphous material was described by combining the differentiated stress optical law with a Maxwell element to produce

$$\frac{d\Delta n_a}{dz} = \frac{C_{op}E}{V}\frac{dV}{dz} - \frac{E\Delta n_a}{V\eta} \tag{10}$$

This approach was first suggested by Nishiumi.[16]

The modified Avrami expression[17-21] was used to model the crystallization kinetics

$$\frac{d\theta}{dz} = \theta_\infty \frac{Kn}{V}\left[\int K/V\,dz'\right]^{n-1}\exp\left(-\left[\int K/V\,dz'\right]^n\right) \tag{11}$$

where the temperature and orientation effects were introduced into the rate determining parameter K according to the suggestions of Magill[22] and Ziabicki[23]

$$K = K_{\max}\exp\left\{-4\ln(2)\left[(T - T_{\max})/D_0\right]^2 + cf_a^2\right\} \tag{12}$$

A number of relationships were needed to describe the physical properties of nylon-66 as a function of temperature, molecular weight, crystallinity, etc. The rheology of nylon-66 was modeled as a Newtonian material

$$\sigma = \eta\frac{dV}{dz} \tag{13}$$

where the elongational viscosity was temperature, molecular weight, and crystallinity dependent. Above T_m an Arrhenius expression was used to describe the temperature dependence

$$\eta = 3.31 \times 10^{-17}(M_n)^{3.5}\exp\left[\frac{7548}{T + 273}\right]\exp\left[4.605\left[\frac{\theta}{\theta_\infty}\right]^{12}\right] \tag{14}$$

while below T_m a WLF expression was used

$$\eta = 1.1 \times 10^{-11}(M_n)^{3.5}\exp\left[\frac{-8.86(T - 100)}{T + 1.6}\right]\exp\left[4.605\left[\frac{\theta}{\theta_\infty}\right]^{12}\right] \tag{15}$$

The last exponential on the right is an empirical expression designed to account for the effect of crystallinity on the elongational viscosity. This term is further discussed below. One would normally expect the molecular weight dependence to be described in terms of M_w, but since the data available in the literature for nylon-66 was given in terms of M_n rather than M_w, M_n was

used in Eqs. (14) and (15). The density of nylon-66 in the melt was given by[24]

$$\rho = [4.86 \times 10^{-4}T + 0.891]^{-1} \tag{16}$$

and below T_m as

$$\rho = \frac{1.1018 - 0.00151\theta}{1 - 0.128\theta} - 4.55 \times 10^{-4}T \tag{17}$$

The specific heat was taken as[25]

$$C_p = 1.4 \times 10^{-3}T + 0.33 \tag{18}$$

Because of the limited amount of available data, the stress optical coefficient and the amorphous and crystalline intrinsic birefringences were taken as constants; $C_{op} = 1.3 \times 10^{-10}$ cm^2/dyne[26] and $\Delta_c^\circ = \Delta_a^\circ = 0.090$.[27] The heat of fusion was 45 cal/g[28] and the ultimate crystalline index was taken as 45%. The parameters in the expression for the crystallization kinetics were for nylon-66; $K_{max} = 1.64\ s^{-1}$, $T_{max} = 150°C$, $D_o = 80°C$,[22] $c = 26{,}000/(T_m - T)$. As no data for stress-induced crystallization of nylon-66 was available in the literature, the value of c was an estimate based on the present experimental data. It was found necessary that c be expressed as a function of supercooling, $T_m - T$.

The ordinary differential equations that comprise the model along with the associated equations describing the material properties were solved simultaneously using a vairable-step fourth-order Runge-Kutta algorithm modified for stiff equations. The solution scheme was facilitated by CSMP (Continuous System Modeling Program), a utility package developed by the International Business Machine Corporation and available through the University of Tennessee Computer Center.

EXPERIMENTAL DETAILS

The nylon-66 used in this investigation was supplied by Monsanto Textiles and Intermediates Company. Intrinsic velocities were obtained for (1) the as-received nylon-66 pellets, (2) pellets which had been dried in a vacuum oven at 115°C for 24 h, and (3) for fiber samples spun under a variety of conditions. These results are summarized in Table I. The number-average molecular weights were computed using the Mark-Houwink coefficients of Taylor.[29] The drying procedure had no effect on the intrinsic viscosity, but there was a significant increase after melt spinning. This increase was attributed to the fact that when nylon-66 is heated in the presence of nitrogen or other antioxidents, it undergoes a chemical reaction at the amine and forms branched structures. In the present study the nylon-66 was stored in prepurified nitrogen after drying and spinning was carried out using a nitrogen purge.

The filaments were melt spun from a Fourne Associates screw extruder with a 13 mm diameter screw. Dried polymer was fed to a nitrogen-purged hopper. The polymer was metered through a gear pump to a single-hole spinneret with

TABLE I
Intrinsic Viscosities of Nylon-66 Samples

Sample	Take-up velocity	Intrinsic viscosity (dL/g)	M_n (g/mol)
Pellet	—	0.96	12,100
Pellet	Dried	0.96	12,100
1	2500	1.19	16,400
2	3500	1.12	15,000
3	4500	1.16	15,800
4	5500	1.22	16,900

a capillary diameter of 635 μm and a length to diameter ratio of 6. The mass throughput was maintained constant at 2.5 g/min and the extrusion temperature was 275°C. Filaments were drawn down at speeds ranging from 2800 m/min to 6600 m/min using a pneumatic-type drawdown device supplied by Rhone Poulenc Fibres. This device is a form of aspirator that uses high velocity air to apply drag forces to the filament and draw it down. It was placed 2.5 m below the spinneret.

Measurements of temperature, diameter, and birefringence as a function of distance from the spinneret were carried out on the running spinline. The temperature profiles were measured with a Barnes infrared microscope using a noncontact, null balance technique described elsewhere.[30,31] The diameter and birefringence profiles were measured using an Olympus polarizing microscope mounted at the appropriate position and angle to the running spinline.[30,31] The actual measurements were made in essentially the same manner that is used for birefringence measurements on stationary filaments that are removed from the spinline. The retardation was measured with a Leitz Berek-type compensator and the filament diameter was measured using a bifilar eyepiece. It was found necessary to use a specially designed guide to steady the filament motion in order to carry out these measurements. It is probable that there is some error introduced by the friction between the filament and the guide. However, by careful adjustment of the guide it is believed that this effect could be rendered quite small. This belief is based on comparison of results obtained in the absence of a guide.

RESULTS AND DISCUSSION

Simulation Results

The simulation was carried out with the processing conditions (i.e., extrusion temperature, mass throughput, spinline length, and take-up velocities) used in the experimental studies of the on-line profiles. The molecular weight of the nylon-66 was chosen to match that of the experimental sample (see Table I). Figure 1 shows the predicted velocity profiles for six take-up velocities. Initially there is a gradual increase in the velocity at each speed. At speeds below 5400 m/min there is a smooth increase in the velocity until the terminal velocity is reached at the take-up device. Above 5400 m/min the velocity increases smoothly to an abrupt plateau, where the velocity increases

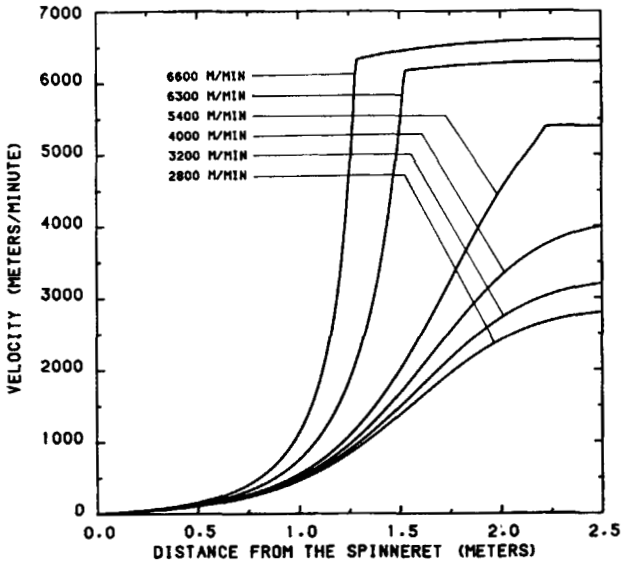

Fig. 1. Predicted velocity profiles for nylon-66 with a mass throughput of 2.5 g/min and $n = 3$.

only slightly thereafter. The distance from the spinneret at which this transition occurs moves closer to the spinneret with further increase in take-up speed. This behavioral transition is due to the strain hardening effect of crystallization taking place within the spinline at the higher speeds.

Figure 2 presents the corresponding diameter profiles. As in the case of the velocity profiles, at speeds below 5400 m/min, the diameter draws down

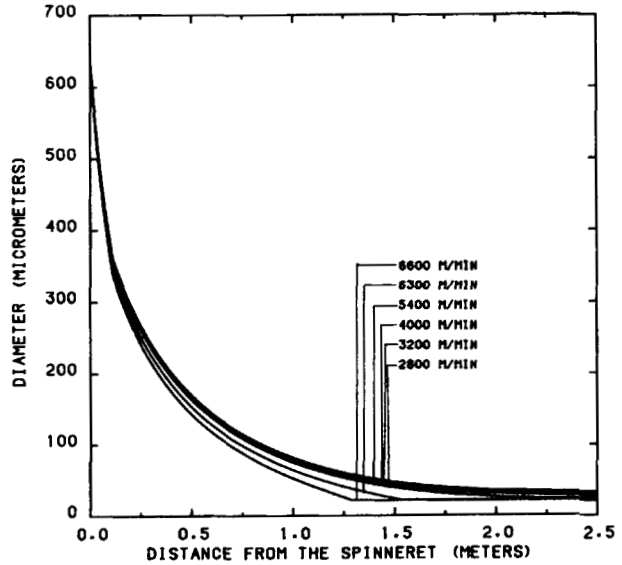

Fig. 2. Predicted diameter profiles for nylon-66 with a mass throughput of 2.5 g/min and $n = 3$.

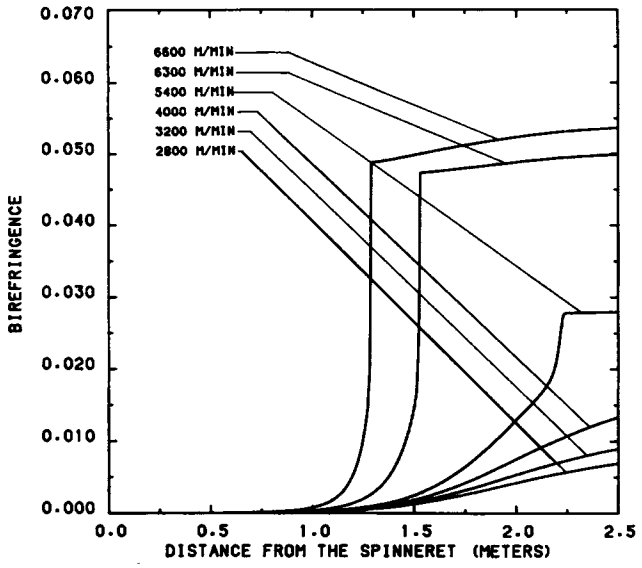

Fig. 3. Predicted birefringence profiles for nylon-66 with a mass throughput of 2.5 g/min and $n = 3$.

smoothly to its final value at the take-up device that would be expected from continuity. Above 5400 m/min the diameter approaches its final value well before the take-up device and remains essentially unchanged from that point on to the take-up device. This is also a consequence of the crystallization taking place within the spinline. The position where the diameter approaches its final value is also the point where the velocity achieves the plateau region.

The predicted birefringence profiles are shown in Figure 3. At low speeds there is a gradual increase in the birefringence, but the final values are rather low compared to the intrinsic birefringences of nylon-66. At higher speeds the birefringence starts out increasing slowly but then rises abruptly, at positions corresponding to the onset of crystallization, to a value very near the final predicted birefringence.

Figure 4 plots the crystalline index profiles at each take-up speed. At low speeds there is no appreciable crystallization taking place in the spinline. This is consistent with the gradual increase and low final values for the birefringence at low spinning speeds. At higher speeds there is a rapid (almost step) increase in the index corresponding to the onset of orientation-induced crystallization that is taking place at positions closer to the spinneret with increasing take-up speed.

Figure 5 shows the predicted temperature profiles. These profiles indicate almost no variation with regard to spinning speed. There is a small temperature plateau at 5400 m/min at about 110°C. This plateau results from the latent heat that is released during crystallization. A much smaller plateau is observed at 6300 m/min, but at significantly higher temperature of about 140°C. It also occurs substantially closer to the spinneret. At higher speeds the orientation-induced crystallization process is proceeding at higher temperatures due to the increased level of molecular orientation at these tempera-

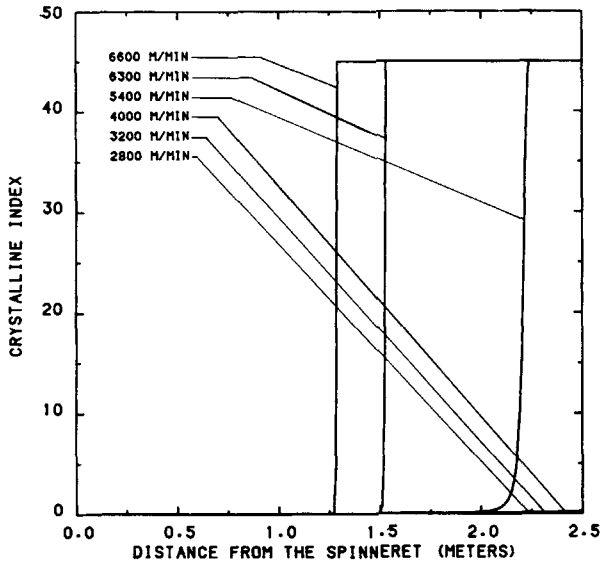

Fig. 4. Predicted crystalline index profiles for nylon-66 with a mass throughput of 2.5 g/min and $n = 3$.

tures. The higher temperatures provide a greater ΔT between the filament and its surroundings which allows the heat of crystallization to be transferred to the surroundings much more efficiently, negating the appearance of a protracted temperature plateau.

The predicted buildup of the stress in the spinline is presented in Figure 6. At the lower speeds the stress within the spinline increases smoothly to its

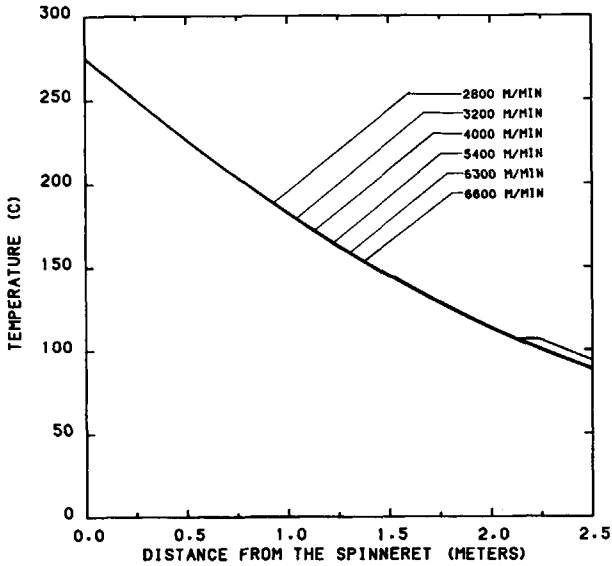

Fig. 5. Predicted temperature profiles for nylon-66 with a mass throughput of 2.5 g/min and $n = 3$.

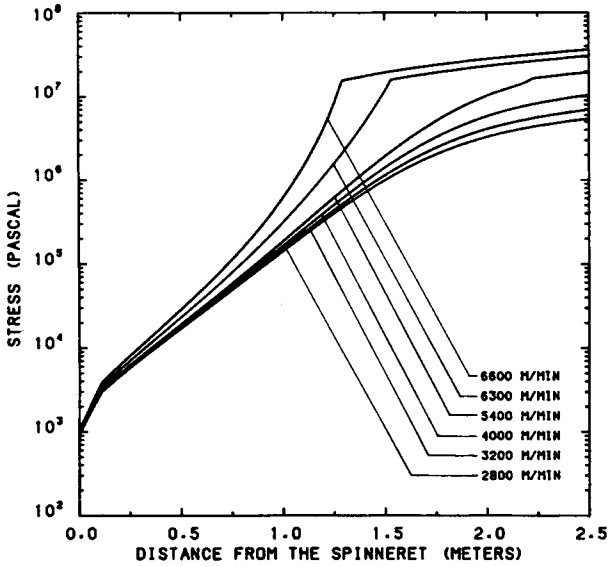

Fig. 6. Predicted stress profiles for nylon-66 with a mass throughput of 2.5 g/min and $n = 3$.

final value at the take-up device. At 5400 m/min the stress increases smoothly to a plateau that corresponds to the point where crystallization occurs. At 6300 and 6600 m/min the stress increases sigmoidally up to the plateau. At all three speeds the crystallization process is initiated when the stress reaches a value of about 2×10^7 Pa. The crystallization rate is greatly enhanced by orientation of the molecules prior to the crystallization process taking place. The driving force for molecular orientation within the spinline is the stress.

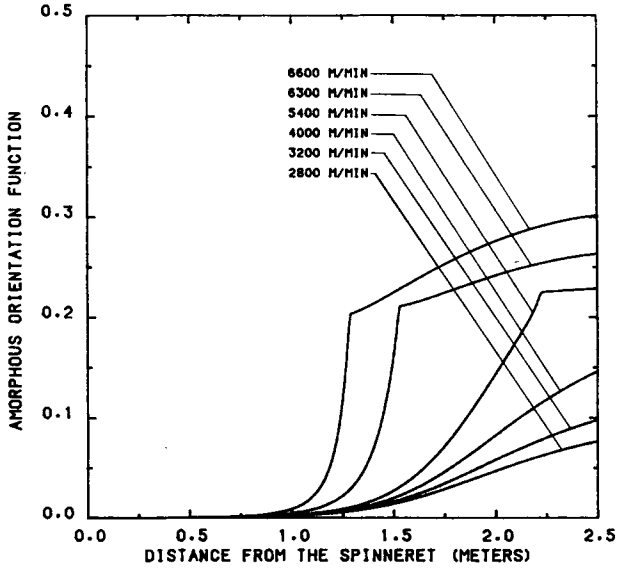

Fig. 7. Predicted amorphous orientation function profiles for nylon-66 with a mass throughput of 2.5 g/min and $n = 3$.

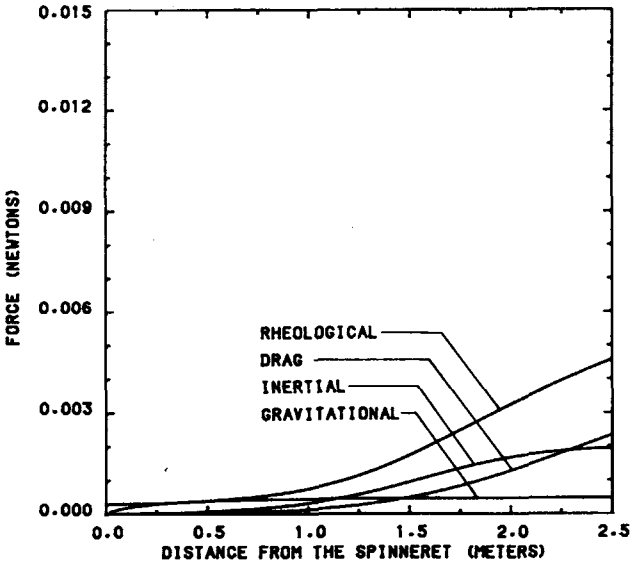

Fig. 8. Predicted rheological, drag, inertia, and gravitational force profiles for nylon-66 at a spinning speed of 2800 m/min.

The model predicts that when a sufficient level of stress (orientation) has been achieved the crystallization process becomes orientation driven rather than temperature driven. This is also demonstrated in Figure 7, where the amorphous orientation factor is small at the low speeds but increases abruptly at the higher speeds to the limit necessary to instigate the crystallization process.

Figures 8 through 10 show the distribution of forces within the spinline as a function of distance from the spinneret. At the lower speeds (Fig. 8) the increase in rheological force is due almost entirely to the acceleration of the fiber until the length of the spinline becomes such that the exposed area of the fiber is great enough so that the drag force becomes significant. In terms of the traditional analyses applied to melt spinning, this regime is a step above the assumption of a constant rheological force. Here the results indicate that inertia and drag become significant only after the fiber has achieved a velocity of around 1000 m/min. Below this speed the rheological force remains essentially constant. Figure 9 indicates the force distribution at 5400 m/min. The acceleration and drag forces combine to increase the rheological force to a level that provides sufficient molecular orientation for a rapid increase in the crystallization kinetics. The force distribution at 6600 m/min (Fig. 10) shows that the increase in the fiber's acceleration alone is sufficient to increase the rheological force to the level necessary to provide the high molecular orientation needed to drive the crystallization kinetics.

The predicted velocity profiles for the same processing conditions, but using a value of one for the Avrami index (n), are shown in Figure 11. Comparing Figure 11 with Figure 1 ($n = 3$) shows no major differences in the character of the profiles. Figure 12 is a plot of the temperature profiles using $n = 1$ in the model. Comparing this with Figure 5 ($n = 3$) shows essentially the same

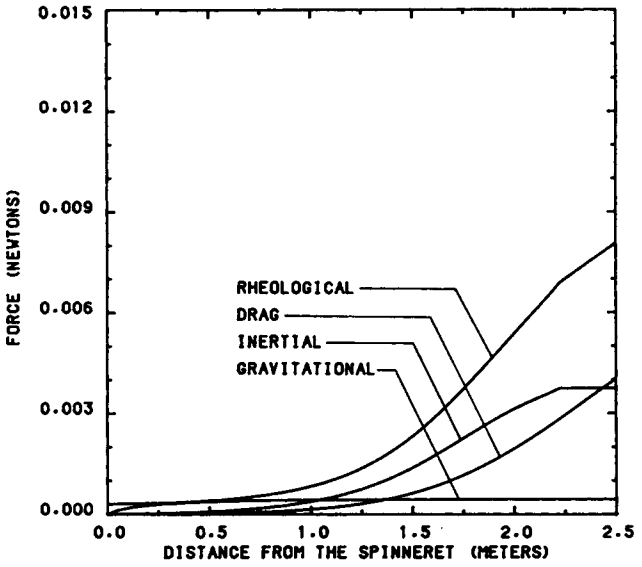

Fig. 9. Predicted rheological, drag, inertial, and gravitational force profiles for nylon-66 at a spinning speed of 5400 m/min.

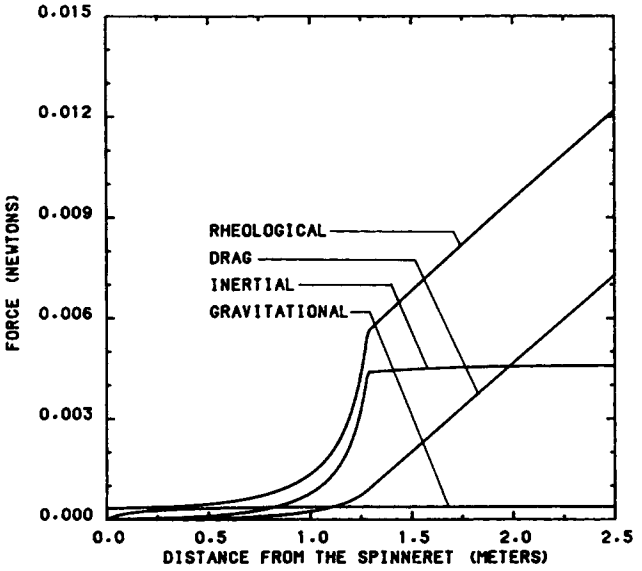

Fig. 10. Predicted rheological, drag, inertial, and gravitational force profiles for nylon-66 at a spinning speed of 6600 m/min.

behavior. The temperature plateaus at 5400 and 6300 m/min appear at almost the same temperature, but are slightly more protracted than those predicted for $n = 3$. There is also a very small plateau in the temperature profile for 6600 m/min. This is a result of the decrease in kinetic rate corresponding to changing n from 3 to 1. Figure 13 shows the crystalline index profiles predicted from the model with $n = 1$. The profiles predicted at the

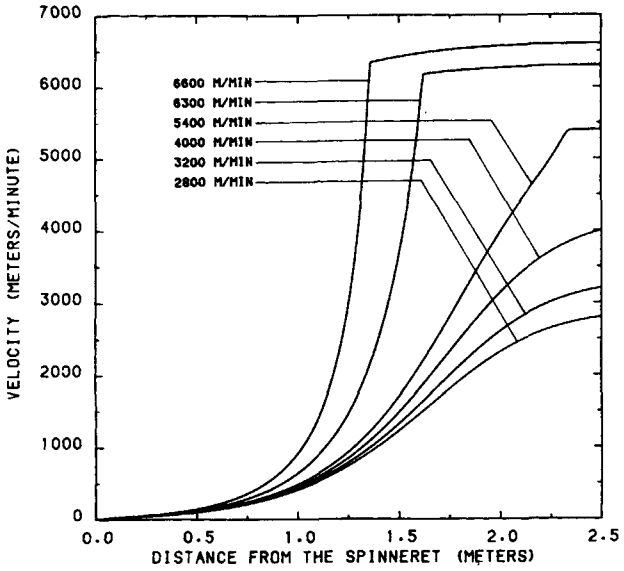

Fig. 11. Predicted velocity profiles for nylon-66 with a mass throughput of 2.5 g/min and $n = 1$.

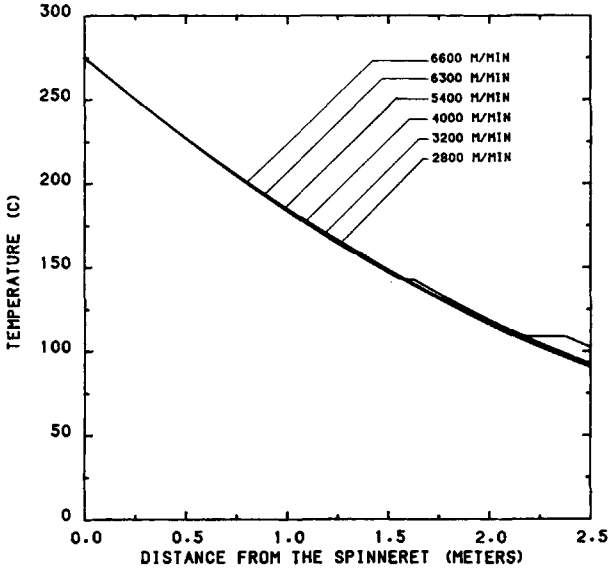

Fig. 12. Predicted temperature profiles for nylon-66 with a mass throughput of 2.5 g/min and $n = 1$.

higher speeds are essentially the same as those predicted with $n = 3$. At the lower speeds the model predicts crystallization will occur, but only to a small extent.

On-line Experimental Results for Nylon-66

The experimental diameter profiles obtained for take-up velocities from 2800 to 6600 m/min are presented in Figure 14. In the range of distances

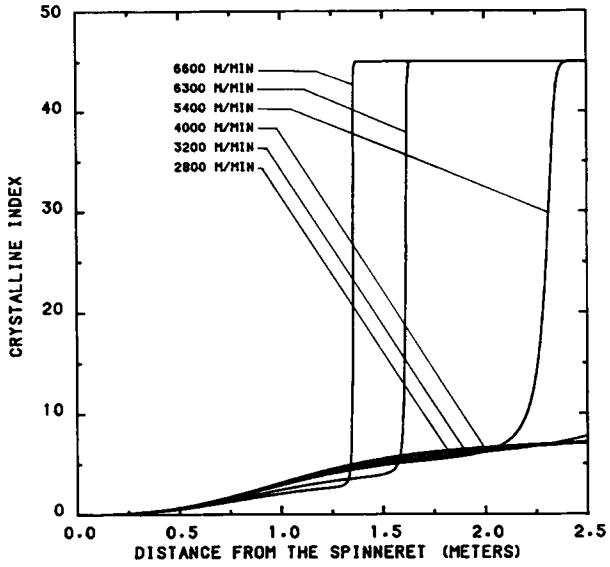

Fig. 13. Predicted crystalline index profiles for nylon-66 with a mass throughput of 2.5 g/min and $n = 1$.

shown, they indicate that, at the lower speeds, the diameter draws down to the final value at the take-up device, but at higher speeds the drawdown occurs much more rapidly and the diameter approaches its final value well before the take-up device.

The experimental birefringence profiles for the same range of speeds as for the diameter profiles are plotted in Figure 15. At low speeds, there is a steady increase from the die exit to the take-up. The profiles at the higher speeds

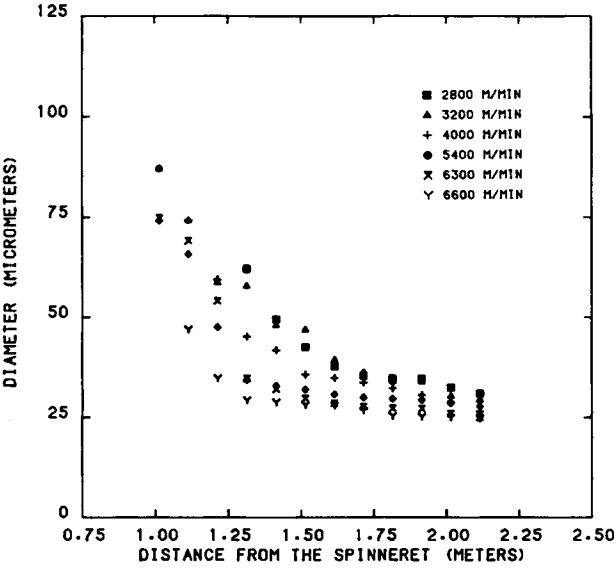

Fig. 14. Experimental diameter profiles for nylon-66 with a mass throughput of 2.5 g/min. m/min: ■, 2800; ▲, 3200; +, 4000; ◆, 5400; ✕, 6300; Y, 6600.

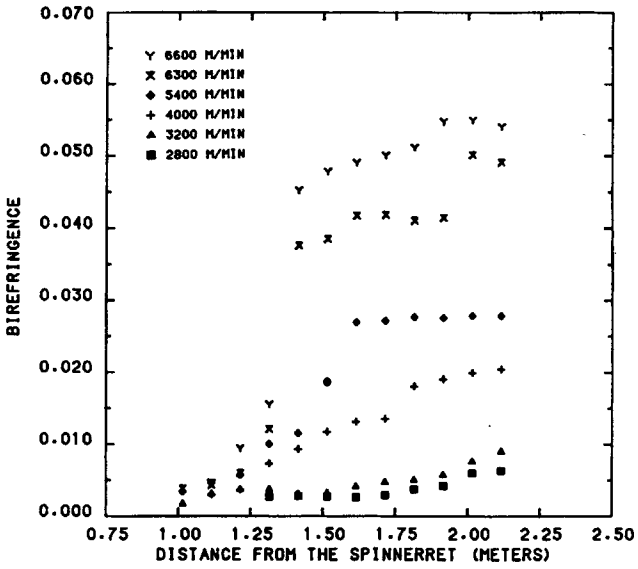

Fig. 15. Experimental birefringence profiles for nylon-66 with a mass throughput of 2.5 g/min. m/min: Y, 6600; X, 6300; ◆, 5400; +, 4000; ▲, 3200; ■, 2800.

indicate a sharp rise in the birefringence up to a plateau region where the birefringence remains until the take-up device is reached. Typical experimental temperature profiles are shown in Figure 16.

Comparison of Model Predictions and On-line Experimental Profiles

Figures 17 and 18 are comparisons between the experimentally obtained diameter profiles and predicted profiles using values of 1 and 3 for the Avrami index, respectively. There are no significant differences between the quality of fit to the experimental data for profiles predicted by the different indices. This may be a result of the relatively high crystallization kinetics of nylon-66 and other inadequacies in the model and the experimental data. The effect of varying the index is most noticeable at the intermediate take-up speeds. This is also apparent in the comparison between the experimental and predicted birefringence profiles (Figs. 19 and 20) for the different Avrami indices. At the lower take-up speeds the crystallization kinetics remain essentially temperature driven, while at the highest speeds the orientation effects overwhelm the temperature influence. At the intermediate speeds they both exert an influence on the kinetic rate.

Figure 21 is a comparison of the diameter profiles predicted by the model with $n = 1$ and substituting 2 for 12 in the equation for the crystallinity effect on the elongational viscosity and the experimentally obtained profiles. The diameter draws down slightly faster than experimentally observed at the highest spinning speeds, this being a consequence of the increased strain hardening effect. Figure 22 compares the predicted and experimental birefringence profiles. The abrupt rise in birefringence at the highest speeds appears nearer the spinneret when the exponent is reduced from 12 to 2. This is also a

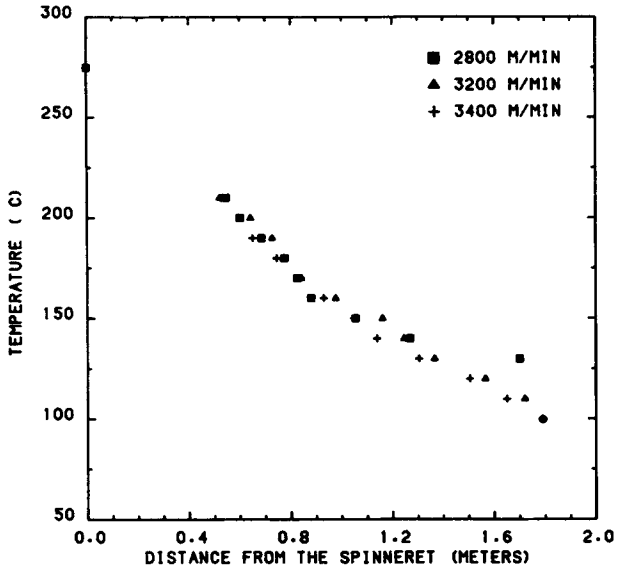

Fig. 16. Experimental temperature profiles for nylon-66 with a mass throughput of 2.5 g/min. m/min: ■, 2800; ▲, 3200; +, 3400.

result of the increased strain-hardening effect. The increase in elongational viscosity causes higher stresses within the fiber which, at the same spinning speed, results in faster diameter drawdown and higher molecular orientation than predicted in the case where the exponent was 12. It is this higher molecular orientation that triggers the crystallization process at positions nearer the spinneret. The predicted crystalline index profiles (Fig. 23) demon-

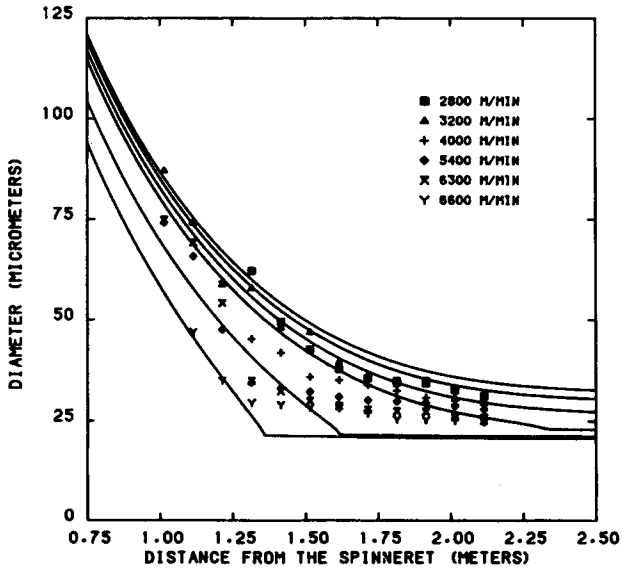

Fig. 17. Comparison of predicted and experimental diameter profiles for nylon-66 with $n = 1$. m/min: ■, 2800; ▲, 3200; +, 4000; ◆, 5400; X, 6300; Y, 6600.

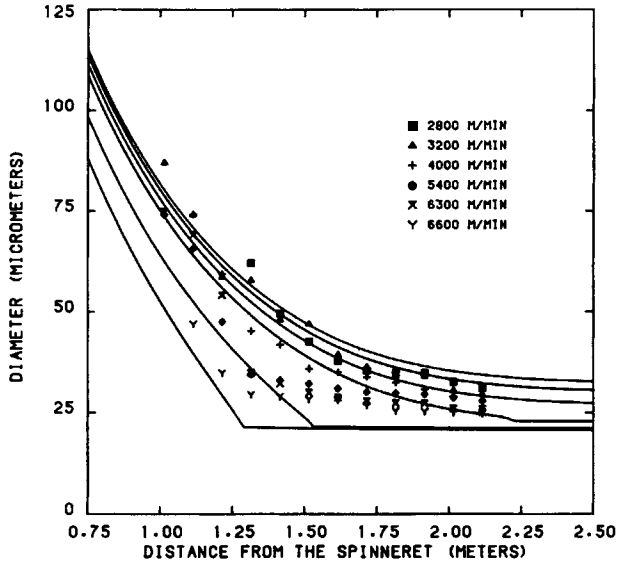

Fig. 18. Comparison of predicted and experimental diameter profiles for nylon-66 with $n = 3$. m/min: ■, 2800; ▲, 3200; +, 4000; ◆, 5400; X, 6300; Y, 6600.

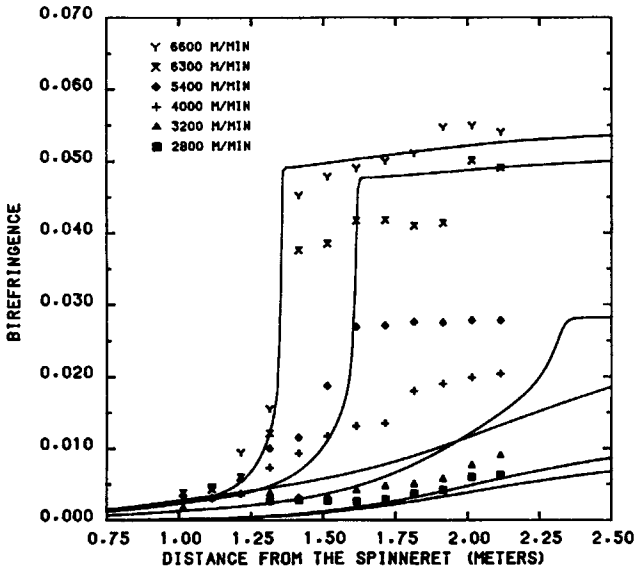

Fig. 19. Comparison of predicted and experimental birefringence profiles for nylon-66 with $n = 1$. m/min: Y, 6600; X, 6300, ◆, 5400; +, 4000; ▲, 3200; ■, 2800.

strate this result. There was little effect on the predicted temperature profiles (Fig. 24) since the crystallization rate of nylon-66 is already quite high.

Discussion

From a comparison of the experimental and predicted profiles it is apparent that the model provides a good semiquantitative description of the process,

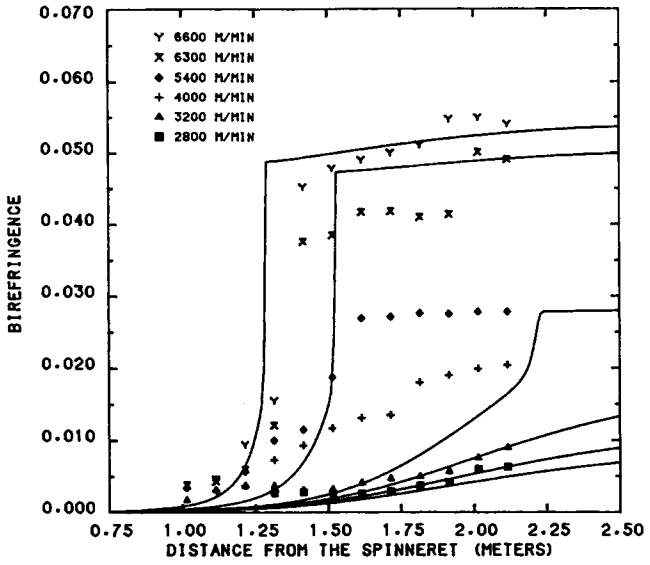

Fig. 20. Comparison of predicted and experimental birefringence profiles for nylon-66 with $n = 3$. m/min: Y, 6600; X, 6300; ◆, 5400; +, 4000; ▲, 3200; ■, 2800.

but there does not exist a one to one quantitative correspondence. This is due to a combination of experimental errors incurred during the data collection procedures, inaccuracies in the physical properties input to the model, and constraints imposed on the model during its development. The most severe limit imposed on the model is neglecting variations across the fiber radius. This was necessary to convert the formulation from a two-dimensional system

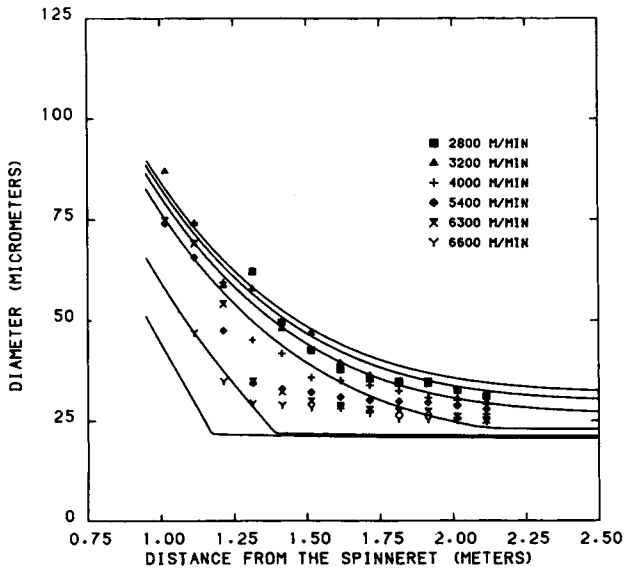

Fig. 21. Comparison of predicted and experimental diameter profiles for nylon-66 using a value of 2 for the exponent in the relationship for the crystallinity on the elongational viscosity. m/min: ■, 2800; ▲, 3200; +, 4000; ◆, 5400; X, 6300; Y, 6600.

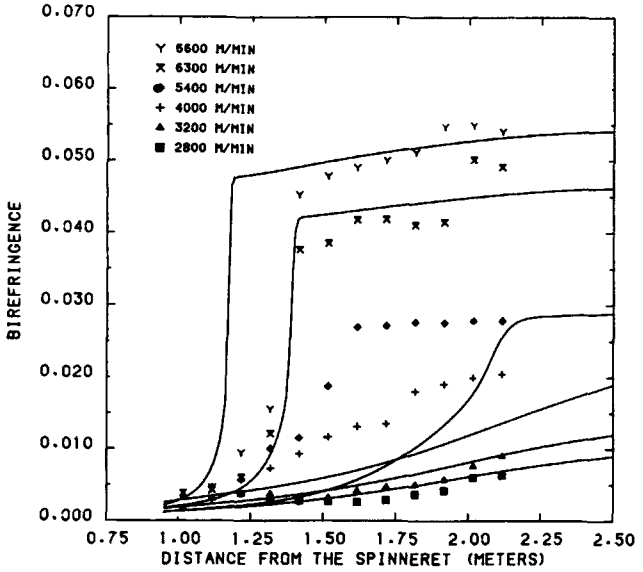

Fig. 22. Comparison of predicted and experimental birefringence profiles for nylon-66 using a value of 2 for the exponent in the relationship for the effect of crystallinity on the elongational viscosity. m/min: Y, 6600; X, 6300; ◆, 5400; +, 4000; ▲, 3200; ■, 2800.

of partial differential equations to a set of ordinary differential equations which could then be solved numerically. This assumption has a series of implications.

The force balance includes the force caused by the friction between the moving fiber and the stagnant air. The net effect of applying the "one-dimensional" assumption is to transfer that contribution from exerting shear at the

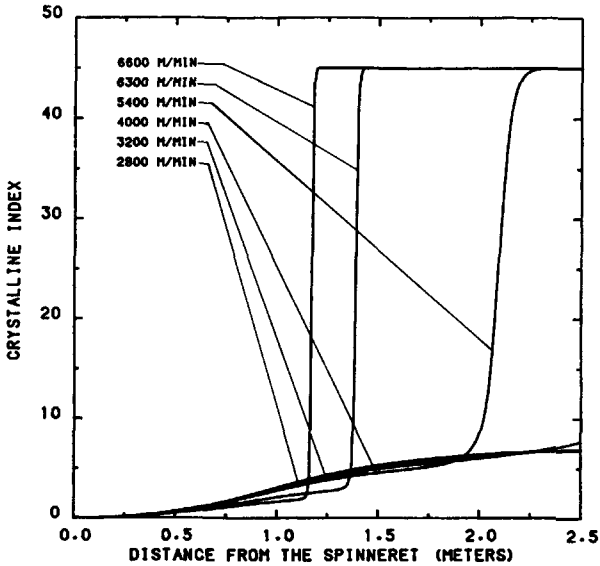

Fig. 23. Predicted crystalline index profiles for nylon-66 using a value of 2 for the exponent in the relationship for the effect of crystallinity on the elongational viscosity.

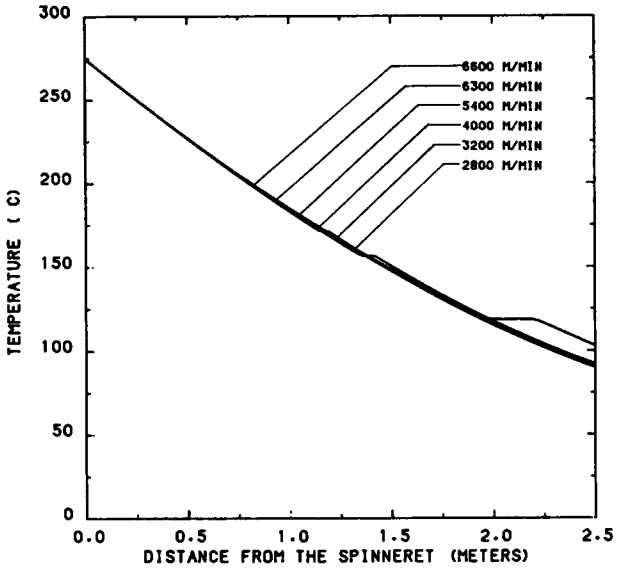

Fig. 24. Predicted temperature profiles for nylon-66 using a value of 2 for the exponent in the relationship for the effect of crystallinity on the elongational viscosity.

fiber surface to increasing the force responsible for uniaxial elongation across the radius. This assumption means that the temperature and orientation are uniform across the radius. With the force and temperature uniformly distributed across the radius the deformation across the radius will also be uniform. The crystallization process will also occur uniformly across the radius since the temperature and orientation are uniform. In the characterization of several polymers spun at high speeds it has been found that under certain spinning conditions there are differences in the structure across the radius, leading to a skin-core effect.[32-35] The skin has a higher orientation and crystallinity than the interior core of the fiber. The present model is unable to deal with these observations.

The molecular orientation of the amorphous material was determined by the birefringence. The relationship that described the birefringence in the model was a combination of the stress optical law and a Maxwell element. This provided a means of computing the change in birefringence along the spinning path. This method, along with neglecting radial variations, means that the molecular orientation of all the amorphous material at a given distance from the die would be the same. This would occur even when some of the amorphous material would be converted during crystallization. There was no mechanism to account for the depletion of the oriented amorphous material during crystallization along the spinning path. The average orientation of the growing crystals was assumed to be the same for all spinning conditions. A more conceptually satisfying alternative would be to describe the orientation of the amorphous and crystalline materials in terms of distributions that are linked to each other by the crystallization kinetics. Abhiraman[36] has attempted to perform an analysis along these lines but the relationships he derived involve several questionable assumptions and would need several more to modify them enough so that they could be incorporated into the present framework.

Even with the incorporation of orientation distributions there still remains the question of how to describe the temperature and orientation effects on the crystallization kinetics. The formulation used in this study is a result of empiricism (temperature dependence) and a simplified theoretical development (orientation effects) by Ziabicki.[23] This is due in part to the large difficulties associated with designing an experiment to actually study the crystallization kinetics of an oriented material and maintain and completely characterize that orientation during crystallization. Add to that the lack of a fundamental theoretical basis for the nucleation and growth phases of the crystallization process in oriented polymers. Even in terms of the simplified Avrami expression used here, there is the possibility of the changing of mechanisms (as indicated by a varying Avrami index) as the velocity increases.

The final limitation in the model involves the characterization of the material itself. A Newtonian constitutive equation was chosen because it is the simplest form and there is enough information available in the literature to be able to incorporate it into the framework. Even in this simplest case there are some questions regarding the best means of incorporating the temperature, molecular weight, and crystallinity effects into an expression for the elongational viscosity. There are no data available on the variation of the elongational viscosity with the elongation rate or molecular weight distribution for the range of temperatures and elongation rates that are commonly found in melt spinning. Since the polymer experiences such a diversity of conditions it is quite difficult to quantitatively describe, using any available constitutive equation, how the polymer will respond to them all. This situation exists for many of the physical properties such as densities, stress optical coefficients, specific heats, and so on of many common materials. Even in the face of all these difficulties, the model does a remarkable job of predicting the behavior of nylon-66 when spun at high and low speeds. The discrepancies appear at those intermediate speeds where one factor does not play a dominant role in determining the overall behavior of the spinline. At the intermediate speeds, there seems to be an interaction or synergism of several factors that the model fails to describe adequately. This does not render the model useless, however. The model, as developed, could be used as a tool to evaluate alternative expressions for the crystallization kinetics or to evaluate the various kinetic parameters by trial and error comparisons with experimental data. It can also be used to simulate a wide variety of processing conditions along with the addition of cooling or heating chambers positioned at various points along the spinline without carrying out time-consuming and expensive experiments.

The strain hardening in the model is manifest in the crystallinity dependence of the elongational viscosity. The form of this dependence was adapted from the form that was used by Kikutani[37] since there was no other data regarding this interaction available in the literature. The strain hardening is a key aspect in the spinning behavior during crystallization and it is important that there should be some experimental studies to investigate the effect of crystallinity on the physical properties over the wide temperature range found in melt spinning of some commonly used polymers.

In order to evaluate to what extent the molecular weight and its distribution play a role in the crystallization behavior during spinning, there is a need

for more information on the variation of the physical properties of the polymer itself along with experimental online studies in which molecular weight is varied systematically.

SUMMARY AND CONCLUSIONS

On-line measurements of diameter, temperature, and birefringence were performed on a nylon-66 spinline for a range of spinning conditions. These results show that the on-line development of orientation and crystallinity is quite dependent on spinning conditions, especially spinning speed.

A mathematical model was applied to analyze the spinning process and to calculate profiles that could be compared to the experimentally measured profiles.

In spite of seemingly overwhelming complexities the model developed in this study has demonstrated that it contains the essential features needed to successfully describe, both qualitatively and semiquantitatively, the high speed melt-spinning behavior of nylon-66. Quantitatively accurate predictions from the model will require more accurate values of physical property inputs, especially elongational viscosity and crystallization kinetics parameters.

The authors wish to acknowledge the support of the National Science Foundation for this research through NSF Grant No. CPE 82-13641. Additional support was provided by Monsanto Fibers and Intermediates Company and Rhone Poulenc Fibres, Inc.

APPENDIX
LIST OF SYMBOLS

c	Coefficient of orientation term in rate constant equation	(−)
C_d	Drag coefficient	(−)
C_{op}	Stress optical coefficient	(cm^2/dyne)
C_p	Specific heat	(cal/g-°C)
D	Diameter	(cm)
D_o	Crystallization rate half width	(°C)
E	Modulus	(dynes/cm^2)
F_{drag}	Force due to air friction	(dynes)
F_{grav}	Force due to gravitation	(dynes)
F_{inert}	Force due to acceleration	(dynes)
F_L	Force supplied by take-up device	(dynes)
F_{rheo}	Force within the fiber	(dynes)
F_{surf}	Force due to surface tension	(dynes)
f_a	Amorphous orientation factor	(−)
g	Gravitation constant	(cm/sec^2)
h	Heat transfer coefficient	(cal/g-cm^2-°C)
K	Rate constant	(s^{-1})
K_{max}	Maximum rate constant	(s^{-1})
M_n	Number-average molecular weight	(g/mol)
n	Avrami index	(−)
Re	Reynolds number	(−)
T	Temperature	(°C)
T_a	Ambient temperature	(°C)

T_m	Equilibrium melting temperature	(°C)
T_{max}	Temperature at maximum crystallization rate	(°C)
V	Velocity	(cm/s)
W	Mass throughput	(g/s)
z	Distance from the spinneret	(cm)
ΔH	Heat of fusion	(cal/g)
Δ_c^o	Crystalline intrinsic birefringence	(−)
Δ_a^o	Amorphous intrinsic birefringence	(−)
Δn_a	Amorphous birefringence	(−)
η	Elongational viscosity	(poise)
ψ	Cooling rate	(°C/s)
θ	Crystalline index	(−)
θ_∞	Maximum crystalline index	(−)
ρ	Density of the fiber	(g/cm^3)
ρ_a	Density of the air	(g/cm^3)
σ	Stress	(dynes/cm^2)

References

1. A. Ziabicki, *Kolloid Z.*, **175,** 14 (1961).
2. S. Kase and T. Matsuo, *J. Text. Mach. Soc., Japan*, **18,** 188 (1965).
3. S. Kase and T. Matsuo, *J. Polym. Sci.*, **A3,** 2541 (1965).
4. S. Kase and T. Matsuo, *J. Appl. Polym. Sci.*, **11,** 251 (1967).
5. A. Prastaro and P. Parrini, *Text. Res. J.*, **45,** 118 (1975).
6. H. Yasuda, H. Sugiyama, and Y. Yanagawa, *Sen-I Gakkaishi*, **35,** 370 (1979).
7. D. K. Gagon and M. M. Denn, *Polym. Eng. Sci.*, **21,** 844 (1981).
8. H. H. George, *Polym. Eng. Sci.*, **22,** 292 (1982).
9. H. Yasuda, H. Sugiyama, and S. Hayashi, *Sen-I Gakkaishi*, **40,** 227 (1984).
10. H. Yasuda, H. Sugiyama, and S. Hayashi, *Sen-I Gakkaishi*, **40,** 488 (1984).
11. A. Dutta and V. M. Nadkarni, *Text. Res. J.*, **54,** 35 (1984).
12. A. V. Shenoy and V. M. Nadkarni, *Text. Res. J.*, **54,** 778 (1984).
13. K. Katayama and M-G. Yoon, in *High Speed Fiber Spinning*, A. Ziabicki and H. Kawai, Eds., Wiley-Interscience, New York, 1985, p. 207.
14. J. Shimizu, N. Okui and T. Kikutani, in *High Speed Fiber Spinning*, A. Ziabicki and H. Kawai, Eds., Wiley-Interscience, New York, 1985, p. 173.
15. B. C. Sakiadis, *Am. Inst. Chem. Eng. J.*, **7,** 467 (1961).
16. S. Nishiumi, *Sen-I Kikai Gakkaishi*, **18,** 1974 (1965).
17. M. Avrami, *J. Chem. Phys.*, **7,** 1103 (1939).
18. M. Avrami, *J. Chem. Phys.*, **8,** 212 (1940).
19. M. Avrami, *J. Chem. Phys.*, **9,** 177 (1941).
20. K. Nakamura, T. Watanabe, K. Katayama, and T. Amano, *J. Appl. Polym. Sci.*, **16,** 1077 (1972).
21. K. Nakamura, K. Katayama, and T. Amano, *J. Appl. Polym. Sci.*, **17,** 1031 (1973).
22. J. H. Magill, *Polymer*, **2,** 221 (1961).
23. A. Ziabicki, *Fundamentals of Fiber Formation*, Interscience, New York, 1976.
24. E. Heyman, *Soc. Plast. Eng. J.*, Oct., 37 (1967).
25. E. C. Schule, in *Encyclopedia of Polymer Science and Technology*, **10,** 557 (1969).
26. M. Danford, M.S. thesis, University of Tennessee, Knoxville, 1976.
27. C. G. Cannon, F. P. Chappel, and J. I. Tidmarsh, *J. Text. Inst.*, **54,** 210 (1963).
28. B. Wunderlich, *Polym. Eng. Sci.*, **18,** 431 (1978).
29. G. B. Taylor, *J. Am. Chem. Soc.*, **69,** 635 (1947).
30. K. F. Zieminski, Ph.D. dissertation, University of Tennessee, Knoxville, June 1986.
31. F-M. Lu and J. E. Spruiell, *J. Appl. Polym. Sci.*, in press.
32. J. Shimizu, A. Watanabe, and K. Toriumi, *Sen-I Gakkaishi*, **30,** 35 (1974).

33. J. Shimizu, N. Okui, and Y. Imai, *Sen-I Gakkaishi*, **35,** 405 (1979).
34. J. Shimizu, N. Okui, and T. Kikutani, *Sen-I Gakkaishi*, **37,** 135 (1981).
35. G. Vassilatos, B. H. Knox, and H. R. E. Frankfort, in *High Speed Fiber Spinning*, A. Ziabicki and H. Kawai, Eds., Wiley-Interscience, New York, 1985, p. 404.
36. A. S. Abhiraman, *J. Polym. Sci., Polym. Phys. Ed.*, **21,** 583 (1983).
37. T. Kukutani, Ph.D. thesis, Tokyo Institute of Technology, 1982.

Received July 2, 1987
Accepted September 30, 1987